

Chapter

Energy Efficient Speed Control of Interior Permanent Magnet Synchronous Motor

Olga Tolochko

Abstract

In this chapter, methods for the structural realization of a speed control system for the interior permanent magnet synchronous motor (IPMSM) using the “maximum torque per ampere” (MTA) and “maximum torque per volt” (MTV) optimal control strategies are considered. In the system in constant torque region, is a technique for adapting the speed controller to the presence of the reactive motor torque component, which improves the quality of the transient processes, is proposed. It is also recommended to approximate the dependence of the flux-forming current component on the motor torque by the “dead zone” nonlinearity, which will simplify the optimal control algorithm and avoid solving the fourth-degree algebraic equation in real time. For the speed control with field weakening technique, a novel system is recommended. In this system, the control algorithms are switched by the variable of the direct stator current component constraint generated in accordance with the MTA law: the upper limit is calculated in accordance with the “field weakening control” (FWC) strategy, and the lower limit in accordance with the MTV strategy. The steady-state stator voltage constraint is implemented through the variable quadrature stator current component limitation. The effectiveness of the proposed solutions is confirmed by the simulation results.

Keywords: interior permanent magnet synchronous motor, optimal control, maximum torque per ampere, maximum torque per volt, field weakening control, stator voltage constraint, simulation

1. Introduction

Currently, more attention is being paid to improving the energy efficiency of managing electromechanical plants. The solution for this problem is of particular importance for electric drive systems with autonomous power sources, in particular for electric vehicles, allowing them to increase their mileage between recharges. One of the motors widely used in electric vehicles is the permanent magnet synchronous motor (PMSM).

Depending on the magnets' location in the rotor, PMSMs are divided into motors with surface-mounted magnets (SPMSM—surface permanent magnet synchronous machine) and interior-mounted magnets (IPMSM—interior PMSM). The surface allocation of the magnets prevents the engine from operating at high speed. With

the internal allocation of the magnets, the mechanical strength of the rotor increases, and this defect is eliminated. SPMSM has a symmetrical magnetic system, since the magnetic permeability of air and permanent magnets is practically the same. The electromagnetic system in IPMSM is asymmetric. Hence, IPMSM is a salient pole motor. This leads to the occurrence, along with the active component of the torque, of an additional reactive component, through which it is possible to obtain larger power/weight, torque/current, and torque/voltage ratios.

For IPMSM, optimal control strategies have been developed [1–5]. They increase the energy efficiency of electric drives in steady-state conditions by forming the relationship between the stator current orthogonal components, corresponding to the chosen optimality criterion.

With IPMSM speed control, three ranges are possible, each with different control algorithms. The greatest difficulty in the practical implementation of such systems is the organization of control switching from one algorithm to another while maintaining stator current and voltage constraints.

There are different approaches to improving the energy efficiency of the studied electric drive systems. First of all, they differ in the kind of losses that are subject to minimization.

Losses in IPMSM frequency systems consist of losses in windings (copper losses), losses in magnetic conductor (iron losses), losses from higher harmonics in windings and grooves (stray losses), switching losses in the frequency converter, and mechanical losses [6, 7]. In turn, the losses in steel consist of losses for reversal of magnetization (hysteresis losses) and losses from eddy currents, and mechanical losses due to friction losses and losses from air or liquid resistance. The commutation, mechanical, and hysteresis losses are determined by approximate empirical formulas. Therefore, to their analysis, many papers [6–11] are devoted. There are also methods for determining them experimentally [12, 13].

Optimization methods have also different input and output signals in minimizing expressions. For systems of torque and speed control, the most logical is the use of the dependences of the direct and quadrature stator current components on the electromagnetic torque. However, these dependencies are most complex. For example, many of them have the form of equations of the fourth degree, which either have to be solved by iterative methods in real time, or approximated by simpler equations by the least squares method, or represented in the form of precomputed look-up tables (LUTs), the search in which it is performed by interpolation methods. Therefore, optimization equations often are found in the form of dependencies between the components of the stator currents or in the form of the amplitude-phase trajectory of the stator current. In both cases, the quality of transient processes deteriorates.

Minimization of copper losses is provided by the “maximum torque per ampere” (MTA) management strategy, and the “maximum torque per volt” (MTV) strategy minimizes steel losses from eddy currents. These strategies use variable speed ranges in different ranges: MTA for under the rated speed and MTV for over the rated speed.

In [14–16], the static characteristics of the drive using the MTA strategy were analyzed without and with taking into account the saturation of the steel and the demagnetization of the permanent magnets. Based on the analysis performed, a control system is synthesized, in which the speed controller generates a reference to the amplitude of the stator current, and the phase angle is determined from the previously calculated LUT.

It was shown in [17] that in the flux-weakening constant power region, the stator current sometimes becomes uncontrollable in transients because of the current regulator saturation. To eliminate this disadvantage, the authors proposed to

set the reference torque of the motor at the output of the speed controller and use another LUT to calculate the reference peak stator current.

In [18], a comparison of the MTA strategy with such additional control methods of energy efficiency increasing as “constant torque angle” (CTA), “unity power factor” (UPF), “constant mutual flux linkage” (CMFL) and “angle control of air gap flux current phasor” (ACAGF). It is shown that UPF control yields a comparatively low voltage requirement but very low torque/current ratio. On comparing UPF with CMFL control, it should be noted that the voltage requirement for CMFLC is next to UPFC but can produce much higher torque/current ratio, which is quite a bit smaller than using the MTA method.

In [19], an equation of the fourth-order polynomial about the direct component of the stator current is derived, the coefficients of which depend on the torque, velocity, and quadrature current. This equation minimizes the total loss as the sum of copper, iron, and stray losses. The loss minimizing solutions are obtained by a simple numerical approach or using a LUT.

In [20], the MTA control strategy of IPMSM and its flux-weakening control strategy are described. In this chapter, electromagnetic torque and the relationship of the direct and quadrature axis currents can be derived with the curve fitting method directly. The approximation is performed by a second-order polynomial using the method of least squares. In this case, the approximating curve, unlike the approximated one, does not fall into a point with coordinates [0, 0], which reduces the accuracy of regulation in the initial section. Flux-weakening control (FWC) algorithm in this paper is phase shifting. In this case, the system is implemented with two control channels, speed and torque, which complicate the configuration of the system and worsen its dynamic properties.

In [21], a flux-weakening scheme for the IPMSM is proposed. This is done by an additional external voltage regulator of the pulse width modulated (PWM) inverter, which controls the beginning of the flux-weakening and its level.

In [22], a novel field weakening technology of IPMM is described. Here, closed-loop control using the output voltage and feed-forward control with the pre-calculated tables are combined.

In [23], field weakening control of fast dynamics and variable DC-link voltage are achieved by suitable combination of look-up table and voltage feedback controller.

In [24], a voltage-constraint tracking (VCT) field weakening control scheme for IPMSM drives is proposed. The control algorithm is presented in the form of a complicated block diagram with numerous branching and computations. In [25] an approach to minimize the electrical losses of the interior permanent magnet synchronous motors is presented. Two control strategies based on unsaturated and saturated motor model are analyzed. To overcome the problem of parameters unavailable, a procedure is proposed to estimate the parameters of the loss minimization conditions.

In [26], a concept for optimal torque control of IPMSM has been presented. The schema is based on look-up tables, where saturation effects can be considered. A consideration of the permanent magnets' demagnetization effect during flux weakening showed the restrictions between the system parameters.

As the review performed shows, many authors suggest optimizing control systems using pre-calculated tables. The disadvantages of this solution are the reduction of the real-time performance and reliability of the system, increased demands on the amount of processor memory, and the impossibility of adapting the control system to changing parameters and signal disturbances. The use of analytical expressions makes it possible to adapt by on-line identification of the current values of the main parameters. A lot of work is devoted to this problem, for example, [25, 27–31].

Methods based on the use of certain analytical expressions or pre-calculated tables belong to the group “loss model-based control” (LMBC). An alternative for them are the search algorithms, which are most often used in minimizing total losses. Their feature is the measurement of losses or input and output power and the use of iterative methods to find the optimal solution in real time. The search algorithms do not require the knowledge of the motor model and parameters, but in the search process, they have a negative effect on the transients and steady-state values of the controlled coordinates.

This chapter accesses simple speed control field oriented control (FOC) vector systems of IPMSM for constant torque and field weakening operation ranges without using pre-calculated tables, search algorithms, on-line solving of algebraic equations using iterative methods and without the presence of additional control loops. The quality of proposed control systems is investigated via simulation.

The chapter content is structured as follows. In Section 2, the problem is formulated. In Section 3, the IPMSM speed control system in the constant torque operating range is analyzed. In Section 4, speed control system with new field weakening technique is analyzed and designed. Section 5 contains conclusions on the chapter.

2. Problem formulation

For the mathematical description of IPMSM, we use the following symbols: $u_d, u_q, i_d, i_q, \psi_d, \psi_q$ — d - and q -axis voltage, current and flux linkage; L_d, L_q —direct and quadrature stator inductance ($L_d < L_q$); $\Delta L = L_d - L_q$; R —stator resistance; $\tau_d = L_d/R, \tau_q = L_q/R$; ω, ω_e —mechanical and electrical rotor speed; p —number of pole pairs; ψ_{pm} —permanent magnet flux linkage; J —moment of inertia; T —motor torque, T_L —load torque.

The differential equations of IPMSM in the d - q rotating reference frame used in the FOC vector systems synthesis are written as follows:

$$\begin{cases} u_d = i_d R + L_d \frac{di_d}{dt} - \omega_e \psi_q, & \omega_e = p\omega, & \psi_q = L_q i_q, \\ u_q = i_q R + L_q \frac{di_q}{dt} + \omega_e \psi_d, & \psi_d = L_d i_d + \psi_{pm}, \\ T = k_t [\psi_{pm} i_q + (L_d - L_q) i_d i_q], & k_t = 1.5p, \\ J \frac{d\omega}{dt} = T - T_L. \end{cases} \quad (1)$$

Table 1 presents the parameters of two motors with different degrees of magnetic asymmetry, for which the research in this chapter is performed.

The task of energy efficient optimal control is to minimize total losses or one of their kinds. Mechanical and switching losses can be most effectively reduced at the design stage of the frequency converter, the motor and the mechanism. Designing a control system based on loss models, usually allows minimizing the copper losses, iron losses or their sum. This chapter discusses methods based on models of copper losses and iron losses from eddy currents.

During analysis and synthesis, the saturation of steel is not taken into account, the methods for parameters identifying and perturbations estimation are not considered.

The graphs in this chapter are presented in p.u. units: $\bar{y} = y/y_b$. As base values, we used: $T_b = T_r, i_b = T_r / (k_t \psi_{pm}), \omega_b = \omega_r = \pi n_r / 30$, and $u_b = e_r = p \omega_r \psi_{pm}$.

Parameters	Designation	Values 1	Values 2
Rated speed	n_r , rpm	4000	2000
Rated torque	T_r , Nm	1.8	1.67
Permanent magnet flux linkage	ψ_{pm} , Wb	0.0844	0.0785
Moment of inertia	J , kg m ²	0.45×10^{-3}	0.5×10^{-3}
Number of pole pairs	p	3	2
Stator resistance	R_s , Ω	2.21	0.87
d-axis inductance	L_d , mH	9.77	14.94
q-axis inductance	L_q , mH	8.72	22.78

Table 1.
 Specifications of IPMSM.

3. Speed control of IPMSM in constant torque region

The block diagram of the IPMSM, designed according to Eqs. (1), is shown in **Figure 1**. The synthesis of the vector control system is traditionally performed according to the block diagram shown in **Figure 1**, neglecting the rotation EMF feedback and the crosslinks denoted by dashed lines, as well as the reactive component of the electromagnetic torque denoted by the bold line.

When using PI current controllers (PI-CCs), synthesized by the series correction method, the dotted links are usually compensated by adding corresponding links with opposite signs to the output signals of the PI-CCs. If the asymmetry of the motors magnetic system is not taken into consideration, the proportional gain (P-) and the transfer function of the proportional-integral (PI-) speed controller (SC) are calculated by the formulas:

$$k_{sc} = \frac{i_q^*(s)}{\Delta\omega(s)} = \frac{J}{k_t \psi_{pm} \tau_\omega}, \quad W_{sc}(s) = \frac{i_q^*(s)}{\Delta\omega(s)} = k_{sc} \frac{\tau_{\omega i} s + 1}{\tau_{\omega i} s} \quad (2)$$

where $\tau_\omega = 2\tau_i$ and $\tau_{\omega i} = 2\tau_{\omega}$; τ_i —integral time-constants of open speed and current loops.

In the first speed range, the copper losses, proportional to the square of the stator current, are determined as:

$$P_{Cu} = 1.5R i_s^2, \quad i_s^2 = i_q^2 + i_d^2. \quad (3)$$

Then the control problem can be formulated as follows: to find such a relation between the orthogonal components of the stator current, at a given torque, at which the amplitude of the current (2) would be smallest possible. This control strategy is called maximal torque per ampere (MTA).

This optimal control problem is a classical variation task for the conditional extremum, which requires minimizing the expression (3) ensuring the additional torque equation from (1). Such a problem is solved by the Euler-Lagrange method and has a known solution:

$$i_{dMTA} = -\frac{\psi_{pm}}{2(L_d - L_q)} - \sqrt{\frac{\psi_{pm}^2}{4(L_d - L_q)^2} + i_q^2}. \quad (4)$$

In conventional IPMSM FOC system, a reference signal $i_{d0}^* = 0$ is applied to the input of the d-axis stator current (CCd). When implementing the MTA-strategy, the easiest way to take the reference for the q-axis current is from the speed

controller and to obtain a reference to the d-axis current from it is through nonlinear functional transformation (4). A fragment of the block diagram for the comparison of the “zero direct current strategy” and the simplest implementation of the MTA strategy is shown in **Figure 2**, where.

$$W_{CCd}(s) = \frac{(\tau_d s + 1)R}{\tau_i s}, \quad W_{CCq}(s) = \frac{(\tau_q s + 1)R}{\tau_i s}.$$

The effectiveness of the MTA strategy is explained in **Figure 3**, which shows in p.u. units a MTA parabola, calculated using expression (4), equal currents circles (Eq. (3)), and equal torques hyperbolae, calculated according to the equation

$$i_q(i_d, T) = \frac{T}{k_t [\psi_{pm} + (L_d - L_q)i_d]}. \quad (5)$$

The intersection points P_i of these hyperbolae with the MTA trajectory determine the optimal distribution of stator current components for given torque values. Circles with centers at the coordinate system origin, drawn through the P_i points with dashed lines, have radii equal to the total stator currents i_{sMTA} with an optimal distribution of their components.

It can be seen from **Figure 3** that a parabolic MTA trajectory intersects equal torques hyperbolae at an angle of 90° , which provides the minimum possible values

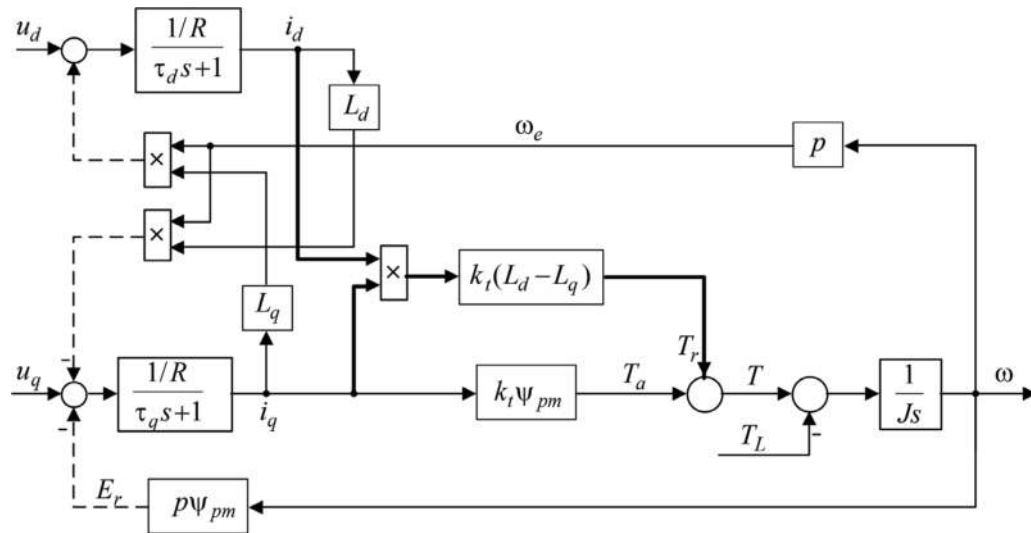


Figure 1. IPMSM block diagram in rotating rotor reference frame.

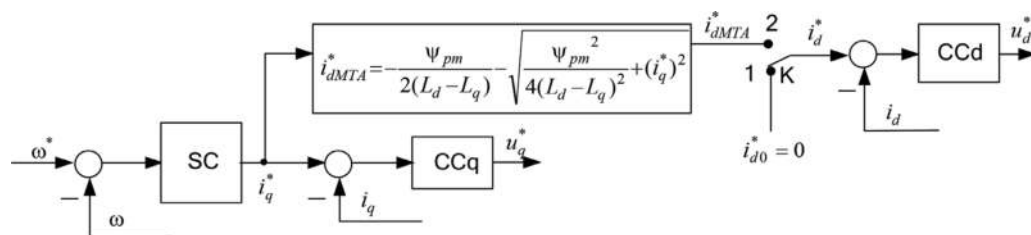


Figure 2. Block diagram for the comparison of the “zero direct current strategy” and the simplest implementation of MTA strategy.

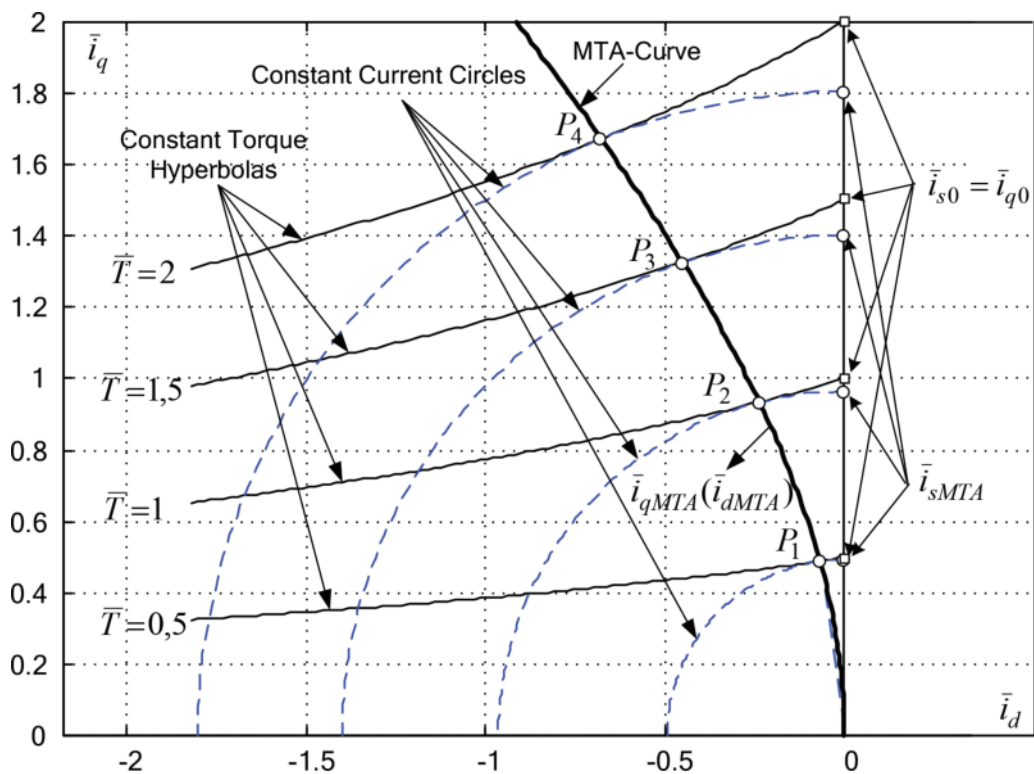


Figure 3.
 Current locus diagram.

of the stator current for a given torque. Therefore, the equal torques hyperbolae lie outside the equal currents circles, that is, any ratio of the orthogonal current components that is different from the optimal one leads to an increase in the modulus of the current vector.

To compare currents when using the control strategies under study, attention should be drawn to the cross points of constant currents circles with the q-axis that defines the current modules for the MTA strategy, and the cross points of constant torques hyperbolae with the same axis that defines the peak current for the strategy “ $i_d = 0$.”

Analysis of the location of these points shows that the advantage of the MTA-strategy increases with increasing electromagnetic torque. This radically differentiates the IPMSM optimal control from the optimal control of induction motor, in which the efficiency of the MTA strategy increases with decreasing electromagnetic torque.

We will perform a study of the static and dynamic properties of IPMSM speed control systems with compared control strategies for the IPMSM with parameters presented in column “Values1” from **Table 1** with time constants $\tau_i = 2\tau_\mu = 0.4$ ms, $\tau_\omega = 2\tau_i = 0.8$ ms.

Transient processes during acceleration with the desired electromagnetic torque without load up to the nominal speed and stepwise load torque response for P-SC are shown in **Figure 4**, and for the PI-SC – in **Figure 5**: (a) with “zero d-current strategy”; (b) with the MTA strategy (Eq. (4)).

From the comparison of the transients, it can be seen that in the conventional control system (a) the torque and current curves practically coincide and have the current and torque overshoot values about 5% during the acceleration of and 10% during step disturbance change in the system with P-SC.

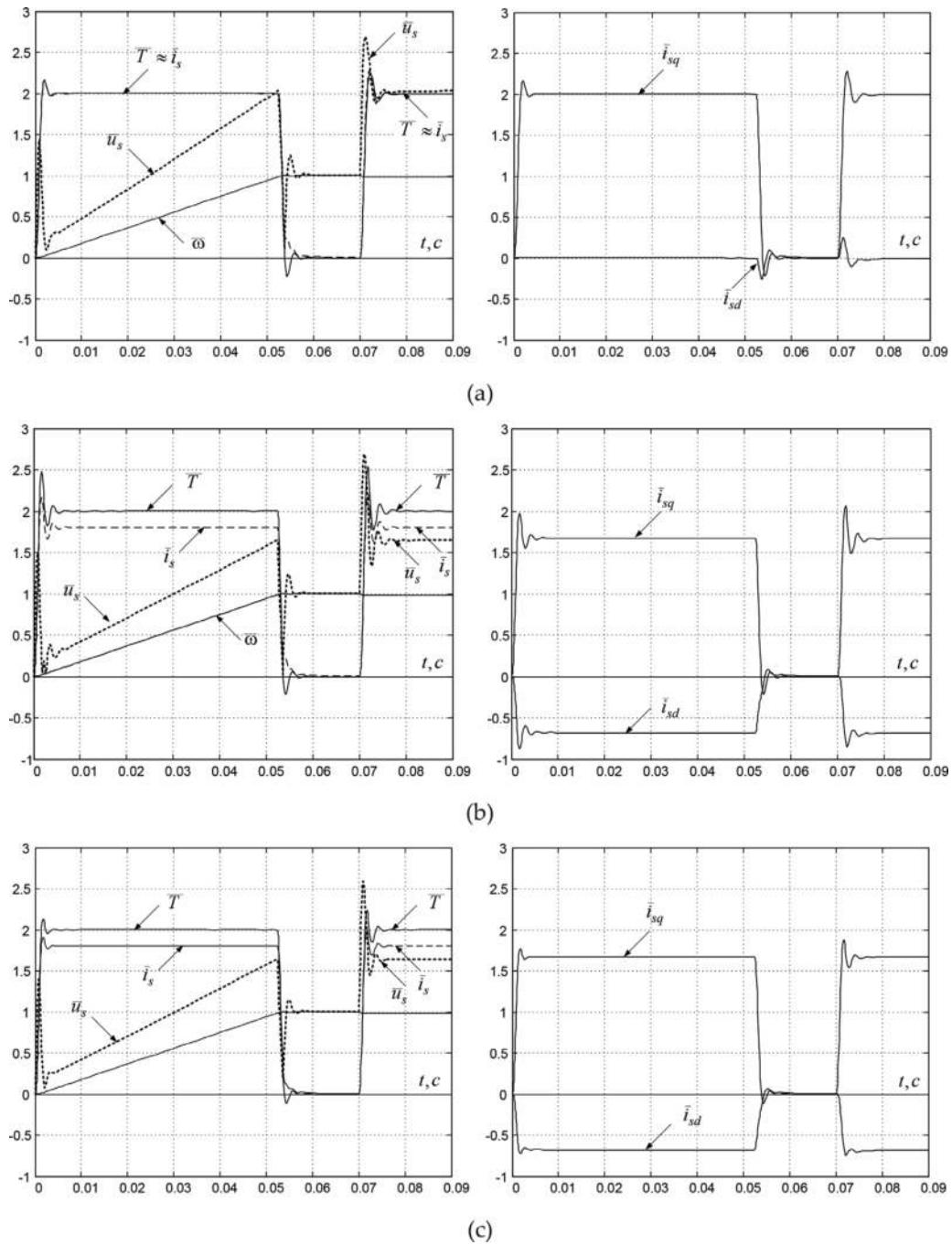


Figure 4. Transients in IPMSM speed control system with P-SC: (a) used strategy $i_d^* = 0$; (b) used MTA strategy with constant P-SC gain; and (c) used MTA strategy with variable P-SC gain.

In the PI-SC system, the corresponding values are 52 and 65%. The dynamic deviations of the d-current from 0 does not exceed 12 and 25% of the rated value. When applying the MTA strategy without changing the setting of SC adjustments (b), the ratio T/i_s increases in steady-state region, but current and torque overshoots increase up to 25% in during the acceleration and to 35% during step disturbance change in the system from P-SC and to 80 and 90% in a system with PI-SC. In this case, the transient oscillation increases significantly.

From the analysis of the block diagram in **Figure 1**, it follows that this shortcoming is due to incomplete plant compensation by the speed controller. Taking

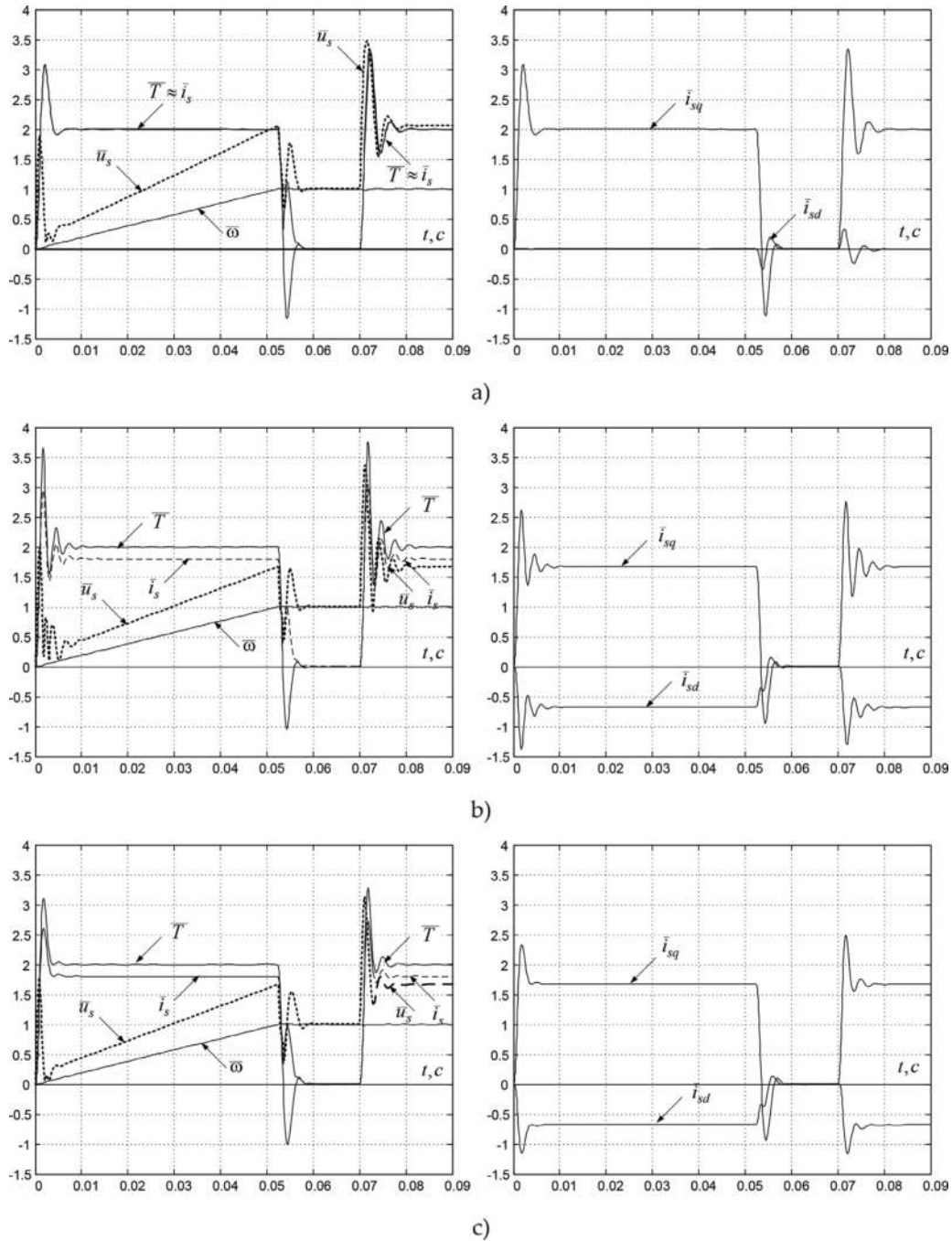


Figure 5. Transients in IPMSM speed control system with PI-SC: (a) used strategy $i_d^* = 0$; (b) used MTA-strategy without SC adaptation; and (c) used MTA strategy with SC adaptation.

into account of the reactive torque, the P-SC must be designed according to the equation

$$k_{sc1} = \frac{J}{\tau_{\omega} k_t [\psi_{pm} + i_d(t)(L_d - L_q)]} = \frac{J}{\tau_{\omega} k_t \psi_d(t)}. \quad (6)$$

Transient processes in the investigated system after the proposed speed controller adaptation to reactive torque effect are shown in the **Figure 4c** and **Figure 5c**. They testify the efficiency of the developed technique, since it significantly reduces

the torque and currents overshoots, as well as overvoltage and transient oscillations without quality loss of the steady-state energy parameters. Correction of the SC (Eq. 6) improves the dynamics of the system but requires putting the division block after the SC.

Let us consider another approach to the MTA algorithm implementation, in which the SC forms the electromagnetic torque reference. In this case, the P-SC gain and the PI-SC transfer function are calculated by the equations:

$$k_{sc2} = \frac{J}{\tau_\omega}, \quad w_{sc2}(p) = \frac{i_q^*(s)}{\Delta\omega(s)} = k_{sc2} \frac{\tau_{\omega i} s + 1}{\tau_{\omega i} s} \quad (7)$$

If we express d-axis current i_d , through torque T and q-axis current i_q from the 4-th equation of the system (1), and substitute the resulting expression into the left-hand side of Eq. (3), then after transformations, we can write an incomplete fourth degree algebraic equation, that reflects the relationship between the electromagnetic torque and the q-axis stator current in an implicit form:

$$i_{qMTA}^4 + \frac{T\psi_{pm}}{k_t(L_d - L_q)^2} i_{qMTA} - \left(\frac{T\psi_{pm}}{k_t(L_d - L_q)} \right)^2 = 0. \quad (8)$$

Eq. (8) can be solved only by numerical methods, which increase the requirements for the microprocessor control devices.

When the system of Eqs. (7), (8) and (4) is used for synthesis, its block diagram acquires the form of **Figure 6**.

To avoid solution of Eq. (8) in real time, the q-axis stator current reference can be calculated using Eq. (5) with $i_q = i_q^*$, $i_d = i_d^*$, and $T = T^*$. In this case, taking into account that, in turn, i_d^* depends on i_q^* , an algebraic loop is formed in a block diagram. This leads to the need to include one sample time delay in the algorithm, as shown in **Figure 7**.

In order to use Eq. (5) in the control algorithm without i_{dMTA}^* signal delay, it is necessary to generate this signal first as a function of the electromagnetic torque. However, the $i_{dMTA}(T)$ dependence is expressed by an even more complicated equation than $i_{qMTA}(T)$:

$$\left(i_{dMTA}^2 + \frac{\psi_{pm}}{(L_d - L_q)} i_{do} \right)^2 + \frac{T\psi_{pm}}{k_T(L_d - L_q)^2} \sqrt{i_{dMTA}^2 + \frac{\psi_{pm}}{(L_d - L_q)} i_{dMTA}} - \left(\frac{T\psi_{pm}}{k_T(L_d - L_q)} \right)^2 = 0. \quad (9)$$

Therefore, we approximate the curve obtained by the numerical solution of Eq. (9). To do this, we analyze the dependence curves of the orthogonal stator current components and peak values of the stator current from the motor torque for

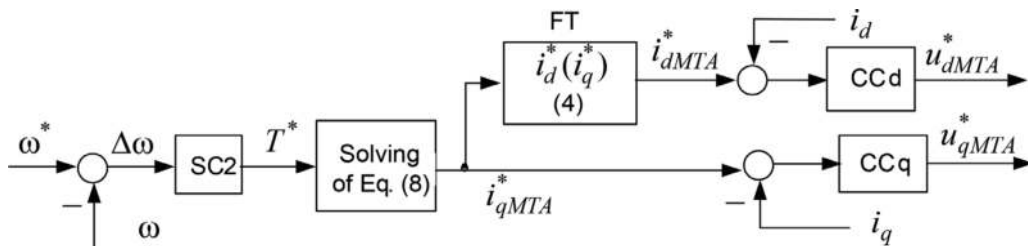


Figure 6. Fragment of the MTA-optimal block diagram, using Eqs. (8), (4) and SC with a gain (7).

the MTA—and “ $i_d = 0$ ”—strategies for the two IPMSMs from **Table 1**, presented in **Figure 8**. In the latter case, the steady-state value of the peak current coincides with its q-component and is determined from the torque equation:

$$i_{q0}(T) = i_{s0}(T) = \frac{T}{k_m \psi_{pm}}. \quad (10)$$

Figure 8 shows that, firstly, the effectiveness of the MTA strategy increases with the increase of the motor torque and its magnetic asymmetry $|\Delta L| = |L_d - L_q|$ and, secondly, the trajectories $i_{dMTA}(T)$ can be linearized quite easily. For the first motor (**Figure 8a**), the difference between the compared strategies with $T \leq 0.5T_r$ is almost nonexistent, and where this difference becomes significant, the plot $i_{dMTA}(T)$ becomes practically linear. Therefore, the dependence calculated by the Eq. (11) can be replaced by the “dead zone” nonlinearity $i_{dMTAk}(T)$ type, which practically does not change the T/i_s ratio:

$$i_{dMTAk}(T) = \begin{cases} 0 & \text{if } |T| \leq T_z, \\ k_l(T - T_z) & \text{if } T > T_z, \\ k_l(T + T_z) & \text{if } T < -T_z, \end{cases} \quad (11)$$

where T_z —dead band limit and k_l —linear gain.

For the second motor, the nonlinear characteristic can generally be approximated by a straight line drawn through the original curve end points. Finding the parameters of the approximating straight by the least-squares method in this case

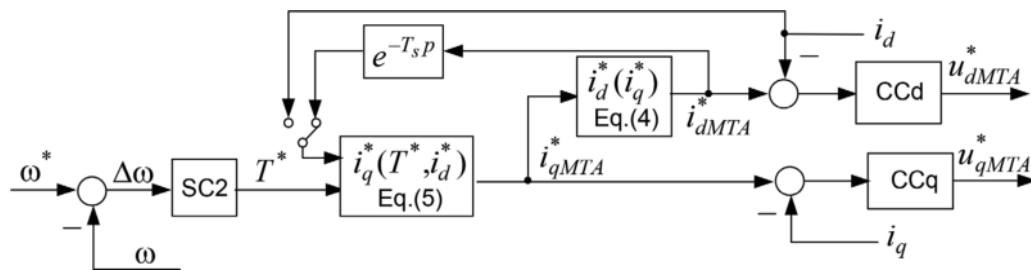


Figure 7. Block diagram fragment using MTA criteria optimization with expressions (4), (5) and delay block.

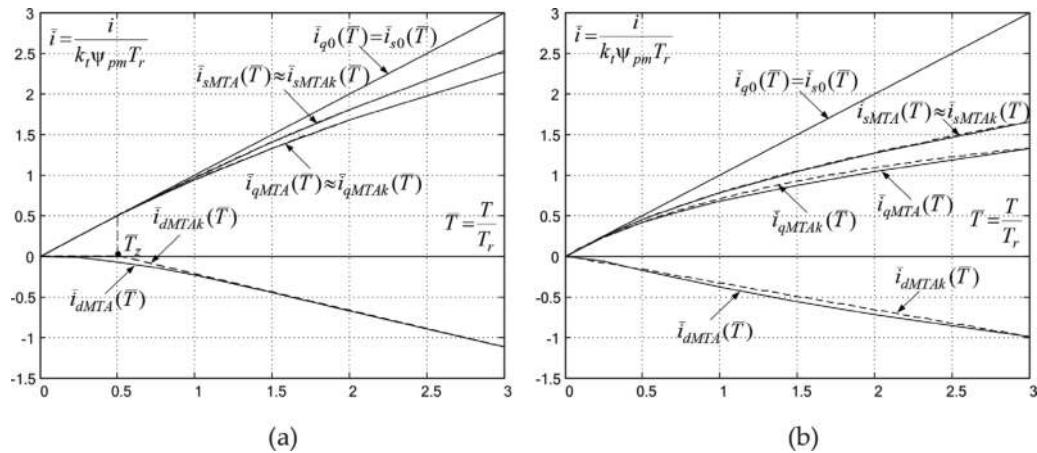


Figure 8. Optimal and quasi-optimal curves $\bar{i}(T)$.

makes no sense, since the goal of the approximation is the minimum deviation from the optimal trajectories of not d- or q-components of the stator current, but its amplitude. The approximations obtained for the nonlinear dependence determined by Eq. (11) can be called quasi-optimal. Their use makes it possible to greatly simplify the system with the implementation of the MTA-strategy, as shown in **Figure 9**.

It is known that when using the MTA strategy, the desired torque value is provided not only with a smaller amplitude of the stator current but also with a lower voltage amplitude of the voltage, which further increases the energy efficiency of the control method in question. The plots of the steady-state voltages are shown in **Figure 10**.

To compare the systems under investigation and to confirm the correctness of the plots in **Figures 8** and **10**, we perform simulation using the example of the second motor from **Table 1**.

Transients are shown in **Figure 11** ($i_d = 0$ -strategy) and **Figure 12** (quasi-optimal MTA strategy (block diagram **Figure 9**)).

Comparison of the transients shows that in the steady state, the values of the currents, voltages, and their components coincide with the values obtained from the static characteristics in **Figure 8b** and **Figure 10b**. Improvement of energy indicators (reduction of current and voltage amplitudes at the same values of torque and speed) occurs without deteriorating the quality of transient processes. The orthogonal components and voltage amplitude decrease not only for steady-state values of the electromagnetic torque but also during its change.

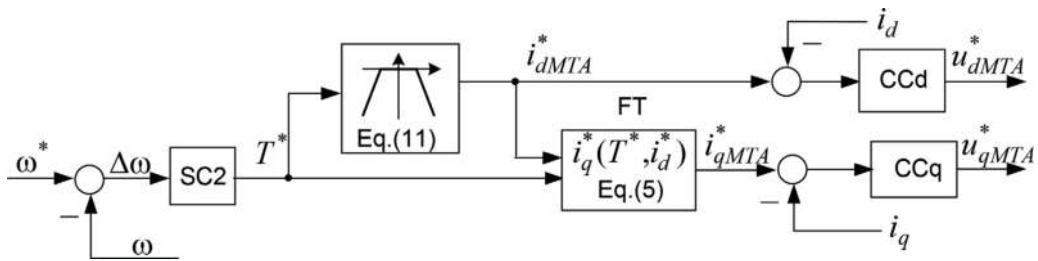


Figure 9.
Block diagram fragment of the MTA-quasi-optimal system.

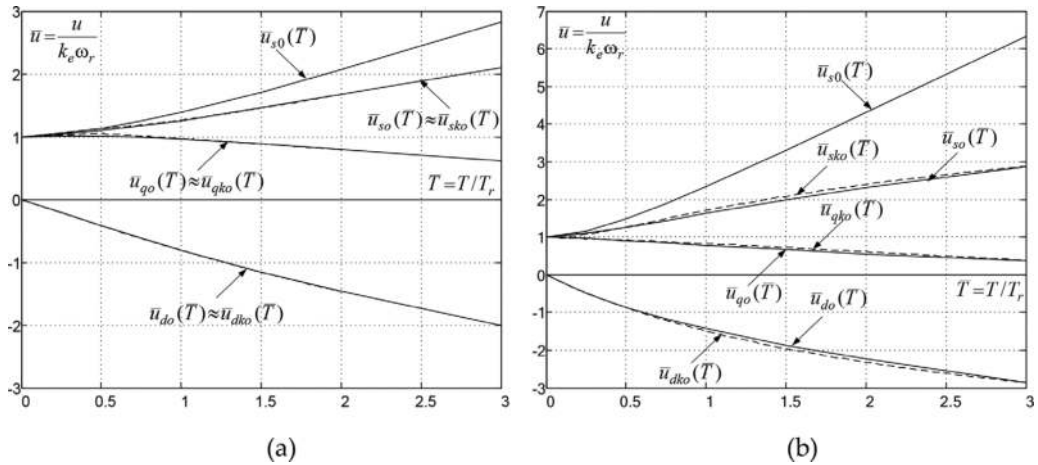


Figure 10.
Optimal and quasi-optimal curves $\bar{u}(T)$.

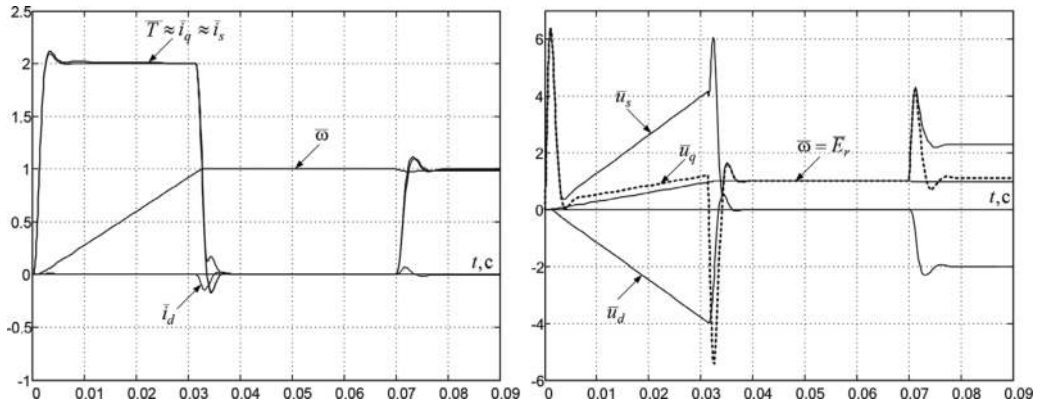


Figure 11.
 Transients in the system used $i_d = 0$ strategy.

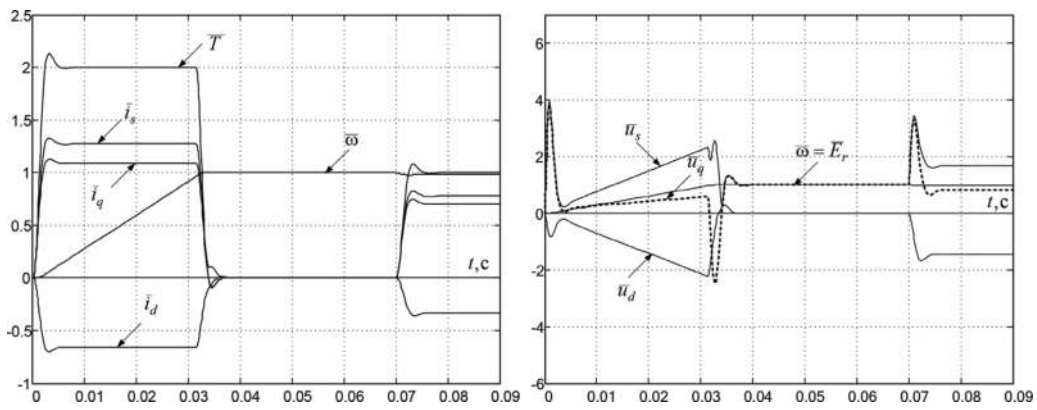


Figure 12.
 Transients in the system used quasi-optimal MTA-strategy.

4. Three-range speed control system of IPMSM

The idea of three-range speed regulation follows from the approximated equation for the peak steady-state stator voltage, which can be obtained from the first two equations of system (1), excluding voltage losses on resistance and inductance:

$$u_s^2 = \sqrt{u_q^2 + u_d^2} \approx \omega_e^2 \sqrt{(L_q i_q)^2 + (\psi_{pm} + L_d i_d)^2}, \quad (12)$$

from where follows:

$$\omega_e \approx \frac{u_s}{\sqrt{(L_q i_q)^2 + (\psi_{pm} + L_d i_d)^2}}. \quad (13)$$

It follows from expression (13) that in the IPMSM, the speed can be increased in three ways:

1. due to a change in the amplitude of the stator voltage from 0 to the nominal value (first range);
2. due to the pseudo-weakening of the permanent magnets field by increasing the d-axis stator current in the negative direction (second range); and

3. due to weakening of the stator field by decreasing the modulus of the q-axis stator current (third range).

The speed control in the first range using the MMA strategy is discussed in the previous section.

The transition to the second range occurs when the stator voltage reaches the nominal value, which is the maximum permissible steady-state voltage value. The relationship between the stator current components in this mode, which is called the field weakening control (FWC), is determined from Eq. (13) with substitutions $u_s = u_{s\max}$ and $\omega_e = \omega_{ep} = \max(\omega_e, p\omega_r)$:

$$i_{dFWC}(i_q, u_{s\max}, \omega_{ep}) = \frac{-\psi_{pm} + \sqrt{u_{s\max}^2/\omega_{ep}^2 - L_q^2 i_q^2}}{L_d}. \quad (14)$$

Substituting (14) into the torque equation, we obtain implicitly the dependence of the q-axis stator current on the torque, voltage, and speed of the motor [1]:

$$i_{qFWC}^4 + p_2 i_{qFWC}^2 + p_1 i_{qFWC} + p_0 = 0, \quad (15)$$

where

$$p_2 = \frac{\psi_{pm}^2 L_q^2 - \Delta L^2 u_{s\max}^2 / \omega_{ep}^2}{L_q^2 \Delta L^2}, \quad p_1 = \frac{4TL_d L_q \psi_{pm}}{3z_p L_q^2 \Delta L^2}, \quad p_0 = \frac{4T^2 L_d^2}{9z_p^2 L_q^2 \Delta L^2}. \quad (16)$$

When adjusting the motor speed in the second range in the current constraint mode, Eq. (16) is modified [1, 2]:

$$i_{dFWC}(i_{s\max}, u_{s\max}, \omega_{ep}) = \frac{-\psi_{pm} L_q + \sqrt{\psi_{pm}^2 L_q^2 - (L_d^2 - L_q^2)(L_q^2 i_{s\max}^2 + \psi_{pm}^2 - u_{s\max}^2 / \omega_{ep}^2)}}{L_d^2 - L_q^2}. \quad (17)$$

As the speed increases, iron losses due to eddy currents become more and more significant:

$$P_{Fe} \approx k_{ec} \psi_s^2 \omega_e^2 \approx k_{ec} u_s^2 = 1.5 \cdot u_s^2 / R_{Fe}, \quad (18)$$

where k_{ec} is the eddy current gain, R_{Fe} is the fictitious resistance of the steel, which is inserted into the motor equivalent circuit to simulate this kind of losses.

This makes it advisable to indirectly limit the iron losses by applying the “maximal torque per volt” (MTV), or the “minimal flux per torque” (MFT) control strategies in the third range. Expressing currents through flux linkages

$$i_d = \frac{\psi_d - \psi_{pm}}{L_d}, \quad i_q = \frac{\sqrt{\psi_s^2 - \psi_d^2}}{L_q}$$

and substituting them into the torque equation, we obtain

$$T = \frac{k_t}{L_d L_q} \sqrt{\psi_s^2 - \psi_d^2} \cdot [L_q \psi_{pm} - (L_d - L_q) \psi_d].$$

Analyzing the last expression for the extremum, we obtain the following equations that ensure the maximum of the torque:

$$i_{dMTV} = \frac{\psi_{dMTV} - \psi_{pm}}{L_d}, \quad i_{qMTV} = \frac{\sqrt{(u_{smax}/\omega_{ep})^2 - \psi_{dMTV}^2}}{L_q}, \quad (19)$$

$$\psi_{dMTV} = \frac{-L_q\psi_{pm} + \sqrt{\psi_{pm}^2 L_q^2 + 8(L_d - L_q)^2 (u_{smax}/\omega_{ep})^2}}{4(L_d - L_q)}.$$

Using the Euler-Lagrange equations to find the minimum of the stator voltage (Eq. (12)), taking into account the torque equation as an additional condition, we obtain the dependence between the components of the stator current for the MTV strategy in the following form:

$$i_{dMTV}(i_q) = -\frac{\psi_{pm}}{2(L_d - L_q)} \cdot \left(2 - \frac{L_q}{L_d}\right) - \frac{L_q}{L_d} \sqrt{\frac{\psi_{pm}^2}{4(L_d - L_q)^2} + i_q^2}. \quad (20)$$

In many papers, the current constraint is achieved by limiting the q-axis stator current at the level:

$$|i_{qmaxi}| = i_q(i_{smax}, i_d) = \sqrt{i_{smax}^2 - i_d^2}. \quad (21)$$

Once again, we emphasize that the MTV strategy is applied in the third range, when the reserves for increasing the speed due to the weakening of the field of permanent magnets are exhausted, and regulation is carried out by decreasing the q-component of the stator current, so that the amplitude of the current also decreases.

The p.u. MTA and MTV trajectories calculated using Eqs. (4) and (20) are shown in **Figure 13**. The same graph shows two constant currents circles of

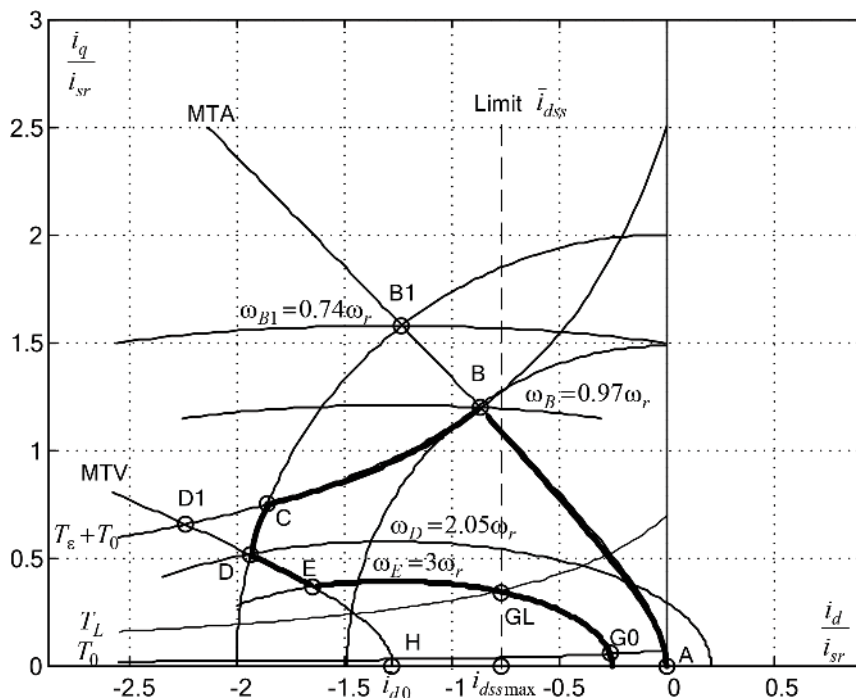


Figure 13.
 Steady-state dq-trajectories of IPMSM.

corresponding to Eq. (21), three constant torques hyperbolae, and three constant velocities ellipses, calculated from Eq. (13) with $u_s = u_{s\max}$.

Acceleration begins from point A via almost instantaneous transition to point B or to point B1 on the trajectory of MTA. With a simultaneous increase in the amplitude and frequency of the stator voltage, the change in speed is not accompanied by a transition to another ellipse. After reaching the nominal voltage amplitude value (point B or B1), which determines the upper limit of this value in the steady state $u_s \leq u_{sr} = u_{s\max}$, the execution of MTA strategy becomes impossible.

Transition from the MTA parabola to MTV parabola occurs either along the maximum allowable current circumference (arch B1-D) or a constant torque hyperbola (hyperbolic line B-D1), or first along the constant torque hyperbola with increase of the current, and then along the overcurrent circumference (path BCD). Movement along the hyperbola is carried out with an underloaded motor with constant torque and voltage. The power increases due to the increase in speed and current. Movement along the circumference occurs at a constant power. These trajectories control the speed in the second range in accordance with the FWC strategy (Eq. 14–17).

Further increase in the speed to the desired value occurs in the third range along the MTV trajectory (Eq. (19)). In this mode (segment D-E), the orthogonal components of the stator current are reduced, resulting in the motor coming out of the current-limiting mode and operating at the reduced values of both stator current amplitude and power.

After the speed has reached its set value, the transition from the acceleration mode to the steady state occurs. In this case, the motion of the working point occurs along an ellipse of constant velocity until it intersects with the load torque hyperbola (segment E-GL or E-G0).

Concentric ellipses of constant velocities have a center at the point H with coordinates $i_{d0} = \psi_{pm}/L_d$, $i_{q0} = 0$, in which the MTV line ends. At this point, a complete demagnetization of the motor takes place, which theoretically makes it possible to achieve an arbitrarily large steady-state velocity ($\omega \rightarrow \infty$) at zero-load torque ($T_L = 0$). In practice, these points are unattainable, and the real range of speed control in the third range is limited by the magnitude of the load torque, the mechanical strength of the rotor, and the constraint of the d-axis stator current in the steady state at about $i_{d0}/2$ to prevent the permanent magnets from being irreversibly demagnetized.

As can be seen from the above Eqs. (4, 5, 8, 9, 14–17, 19–21), a general algorithm for controlling the speed of IPMSM in the three range requires significant computational resources associated with the need for a numerical solution of algebraic equations in real time and complex logic branching for the purpose of organizing controlled switching, etc. Replacing a single algorithm with multidimensional look-up tables of data is associated with the preliminary calculation of a large number of curves and the organization of the search in these tables.

Meanwhile, the analysis of the control trajectories in **Figure 13** suggests the possibility of a structural implementation of the control algorithm, which is presented in **Figure 14**.

In it, the speed controller SC forms the torque reference. To avoid solving fourth-degree algebraic equations in real time (Eqs. 8, 9, 15) and computations according to formulas (19), the q-axis stator current reference is determined by the Eq. (5) with $T = T^*$, $i_q = i_q^*$. To prevent the formation of an algebraic loop, we use in this equation not the reference i_d^* , but the feedback signal i_d .

The limitation of the stator current amplitude is achieved by the dynamic saturation block Sat1 for the q-axis current at the level (21), which is calculated

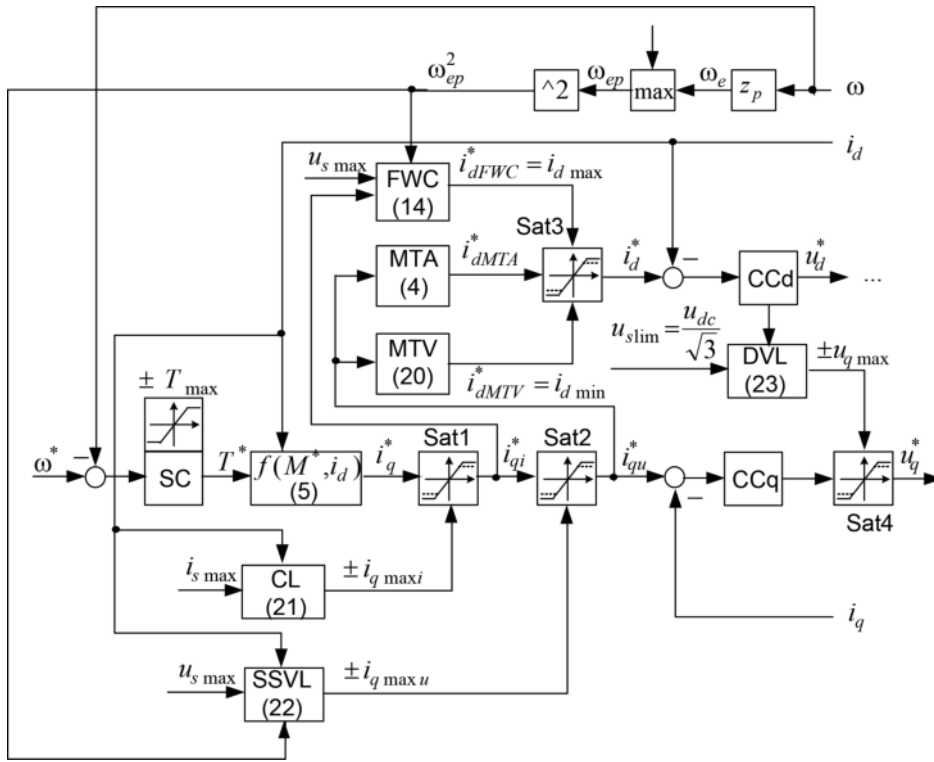


Figure 14. Block diagram of the three-range IPMSM speed control system considering voltage and current constraints.

by current limit block CL. The dynamic saturation block Sat2 for the stator voltage in no-load mode is switched in series with the block Sat1, and the constraint signal is formed by the steady-state voltage limit block SSVL according to the equation

$$i_{q\max u} = \sqrt{(u_{s\max}/\omega_{ep})^2 - (L_d i_d + \psi_{pm})^2 / L_q}, \quad (22)$$

obtained from Eq. (12) at $u_s = u_{s\max}$. Thus, at the output of the block Sat2, we obtain a signal $|i_{qu}| = \min[|i_q|, |i_{q\max i}|, |i_{q\max u}|]$.

To ensure that the motor voltage in dynamic modes does not exceed the inverter DC link voltage, the output of the regulator CCq is limited at the level

$$u_s \leq u_{\lim} = u_{dc} / \sqrt{3} \quad (23)$$

with the blocks of dynamic voltage limit (DVL) and Sat4.

The d-axis current reference signal in the first region is calculated from the Eq. (4) as a function of the signal (22), in the second range from the Eq. (14) as the function of signal (21) and in the third region from the Eq. (20) with the input signal (22). The switching of the control algorithm from MTA to FWC and from FWC to MTV occurs by dynamically limiting the signal of the MTA block at the top level i_{dFWC}^* and at the bottom level i_{dMTV}^* .

Transients in the system shown in Figure 14, obtained via simulation, are shown in Figure 15.

The coordinates of the characteristic points of the transients in Figure 15 coincide with the corresponding points of the diagrams in Figure 13. The stator current does not exceed its maximum permissible value, and the stator voltage in no-load

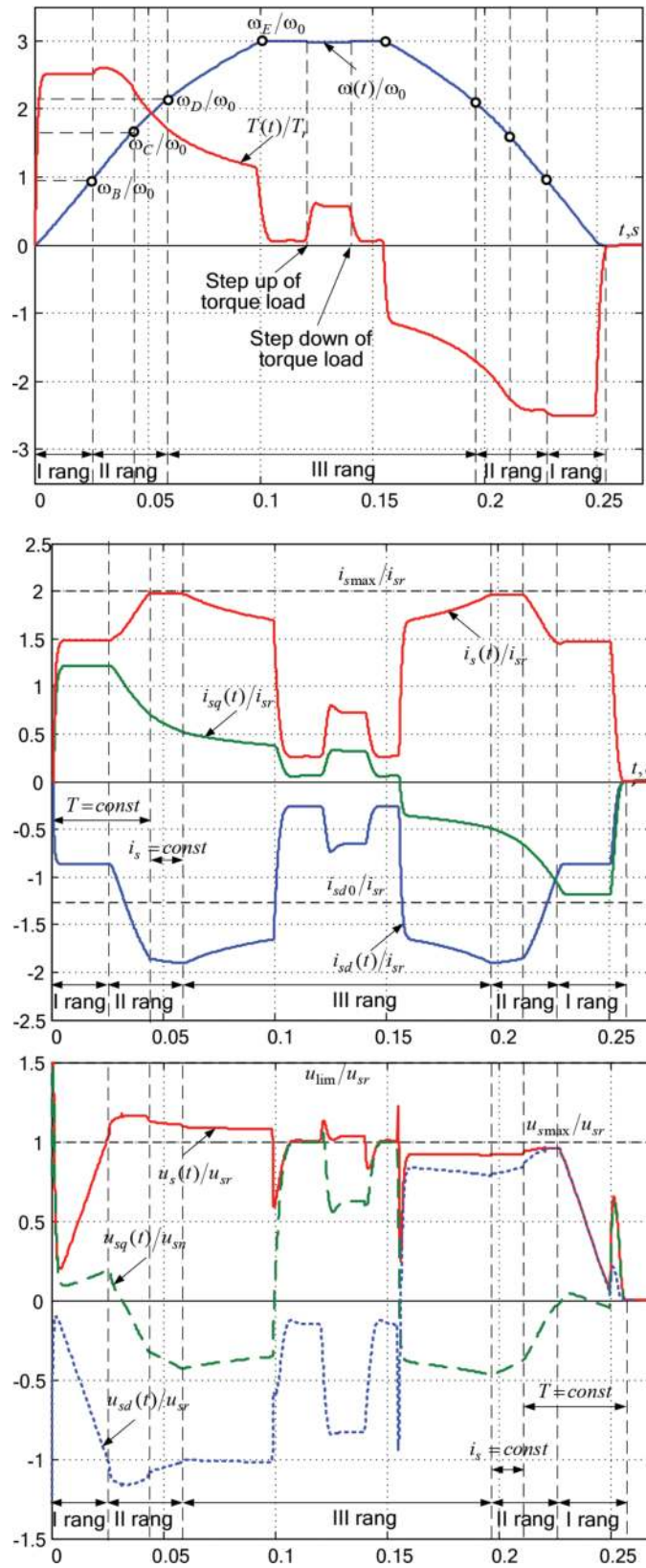


Figure 15.
 Transients in the 3-range speed control system of IPMSM.

mode is equal to the nominal stator voltage, and in dynamic modes, it is limited by the output voltage of the inverter DC link.

5. Conclusions

In this chapter, we presented the IPMSM speed control systems. Two options for improving the quality of the transient processes for the speed regulation by changing the stator voltage using the MTA strategy are proposed. In a system in which the speed controller generates q-axis stator current reference, a method is proposed for adapting the speed controller to the presence of the reactive component of the electromagnetic torque. In a system in which the speed controller forms the electromagnetic torque reference, it is suggested to approximate the dependence $i_d^*(T^*)$ using the “dead zone” nonlinearity and thus avoid solving the fourth-order equation in real time. At the same time, it was possible to ensure high energy parameters without the use of pre-calculated tables and organization of search in them without degrading the quality of transient processes.

For the system with a three-range speed regulation, a system is proposed using MTA, FWC, and MTV strategies with automatic switching between them and stator current and voltage constraints without using additional control loops is proposed.


The analytical researches are confirmed by the simulation results.

Author details

Olga Tolochko
National Technical University of Ukraine, Igor Sikorsky Polytechnic Institute,
Kyiv, Ukraine

*Address all correspondence to: tolochko.ola@gmail.com

IntechOpen

© 2019 The Author(s). Licensee IntechOpen. This chapter is distributed under the terms of the Creative Commons Attribution License (<http://creativecommons.org/licenses/by/3.0>), which permits unrestricted use, distribution, and reproduction in any medium, provided the original work is properly cited. 

References

- [1] Schröder D. Elektrische Antriebe – Regelung von Antriebssystemen. 3. bearbeitete Auflage. Berlin, Heidelberg: Springer; 2009. p. 1336. DOI: 10.1007/978-3-540-89613-5
- [2] Krishnan R. Permanent magnet synchronous and brushless DC motor drives. Virginia Tech, Blacksburg, USA: CRC press; 2010. p. 611. ISBN 978-0-8247-5384-9
- [3] Bose BK. Modern power electronics and AC drives. New Jersey: Prentice Hall PTR; 2002. p. 711. ISBN 0130167436, 9780130167439
- [4] Sul S-K. Control of electric machine drive systems. Willey-IEEE Press; 2011. p. 424. ISBN: 978-0-470-59079-9
- [5] Doncker RD, Pulle DWJ, Veltman A. Advanced electrical drives. Analysis, modeling, control. Berlin: Springer; 2011. p. 455. DOI: 10.1007/978-94-007-0181-6
- [6] Agrawal J, Bodkhe S. Steady-state analysis and comparison of control strategies for PMSM. Modelling and Simulation in Engineering; 2015. p. 11. DOI: 10.1155/2015/306787
- [7] Morimoto S, Takeda Y, Hatanaka K, Tong Y, Hirasaka T. Design and control system of permanent magnet synchronous motor for high torque and high efficiency operation. In: Industry Applications Conference Record of the 1991 IEEE Industry; 1991; 1. pp. 176-181. DOI: 10.1109/IAS.1991.178151
- [8] Morimoto S, Hatanaka K, Tong Y, Takeda Y, Hirasaka T. High performance servo drive system of salient pole permanent magnet synchronous motor. In: Industry Applications Society Annual Meeting of the IEEE Conference Record Proceedings; 1; 28 September–4 October 1991; pp. 463-468. DOI: 10.1109/IAS.1991.178196
- [9] Morimoto S, Sanada M, Takeda Y. Wide speed operation of interior permanent magnet synchronous motors with high performance current regulator. IEEE Transactions on Industry Applications. 1994; **IA-30**(4): 920-926. DOI: 10.1109/28.297908
- [10] Morimoto S, Hatanaka K, Tong Y, Takeda Y, Hirasaka T. Servo drive system and control characteristics of salient pole permanent magnet synchronous motor. IEEE Transactions on Industry Applications. 1993; **29**(2):338-343. DOI: 10.1109/28.216541
- [11] Lee J-G, Nam K-H, Lee S-H, Choi S-H, Kwon S-W. A lookup table based loss minimizing control for FCEV permanent magnet synchronous motors. In: 2007 IEEE Vehicle Power and Propulsion Conference Journal of Electrical Engineering Technology; 9–12 September 2007; Arlington, USA; 4(2). pp. 201-210. DOI: 10.1109/VPPC.2007.4544120
- [12] Huang S, Chen Z, Huang K, Gao J. Maximum torque per ampere and flux-weakening control for PMSM based on curve fitting. In: Vehicle Power and Propulsion Conference (VPPC), 2010 IEEE; 1–3 September 2010; Lille, France. DOI: 10.1109/VPPC.2010.5729024
- [13] Ma L, Sanada M, Morimoto S, Takeda Y. Prediction of iron loss in rotating machines with rotational loss included magnetics. In: IEEE Transactions on Magnetics; 2003. 39(4). pp. 2036-2041. DOI: 10.1109/TMAG.2003.812706
- [14] Li L, Huang X, Baoquan Kao B, Yan B. Research of core loss of permanent

- magnet synchronous motor (PMSM) in AC servo system. In: *Electrical Machines and Systems. ICEMS*; 17–20 October 2008; Wuhan, China. pp. 602–607. INSPEC Accession Number: 10458526
- [15] Navrapescu V, Kisck DO, Popescu M, Kisck M, Andronesu G. Modeling of iron losses in salient pole permanent magnet synchronous motors. In: *7th International Conference on Power Electronics (ICPE '07)*; 22–26 October 2007; Daegu, South Korea. pp. 352–357. DOI: 10.1109/ICPE.2007.4692408
- [16] Urasaki N, Senjyu T, Uezato K. A novel calculation method for iron loss resistance suitable in modeling permanent-magnet synchronous motors. *IEEE Transactions on Energy Conversion*. 2003;**18**(1):41–47. DOI: 10.1109/TEC.2002.808329
- [17] Wijenayake AH, Schmidt PB. Modeling and analysis of permanent magnet synchronous motor by taking saturation and core loss into account. In: *1997 International Conference on Power Electronics and Drive Systems*; 26–29 May 1997; Singapore. DOI: 10.1109/PEDS.1997.627416
- [18] Yan Y, Zhu J, Guo Y. A permanent magnet synchronous motor model with core loss. *Journal of the Japan Society of Applied Electromagnetic and Mechanics*. 2007;**15**:147–150
- [19] Mansouri A, Trabelsi H. On the performances investigation and iron losses computation of an inset surface mounted permanent magnet motor. *Systems, Signals and Devices*. 2012. P. 1–5
- [20] Mi C, Slemo GR, Bonert R. Minimization of iron losses of permanent magnet synchronous machines. *IEEE Transactions on Energy Conversion*. 2005;**20**:121–127. DOI: 10.1109/TEC.2004.832091
- [21] Kim J.-M., Sul S.-K. Speed control of interior permanent magnet synchronous motor drive for the flux weakening operation. In: *IEEE Transactions on Industry Applications*, Vol. 33, No. 1, January/February 1997. p. 43–48. DOI: 10.1109/28.567075
- [22] Bae B-H, Patel N, Schulz S, Sul S-K. New field weakening technique for high saliency interior permanent magnet motor. In: *38th IAS Annual Meeting on Industry Applications Conference*, 2003; 12–16 October 2003; Salt Lake City, USA. pp. 898–905. DOI: 10.1109/IAS.2003.1257641
- [23] Lee JH, Lee JH, Park JH, Won CY. Field-weakening strategy in condition of DC-link voltage variation using on electric vehicle of IPMSM. In: *Electrical Machines and Systems (ICEMS)*. 20–23 August 2011; Beijing, China; 2011. 27 Jan/Feb. pp. 38–44. DOI: 10.1109/ICEMS.2011.6073676
- [24] Sue S-M, Pan C-T. Voltage-constraint-tracking-based field-weakening control of IPM synchronous motor drives. In: *IEEE Transactions on Industrial Electronics*; 55(1); January 2008. pp. 340–347. DOI: 10.1109/TIE.2007.909087
- [25] Hao S, Shi J, Hao M, Mizugaki Y. Closed-loop parameter identification of permanent magnet synchronous motor considering nonlinear influence factors. *Journal of Advanced Mechanical Design, Systems and Manufacturing*. 2010;**4**(6):1157–1165. DOI: 10.1299/jamdsm.4.1157
- [26] Meyer M, Bocker J. Optimum control for interior permanent magnet synchronous motors (IPMSM) in constant torque and flux weakening range. In: *Power Electronics and Motion Control Conference, 2006. EPE-PEMC 2006. 12th International Power Electronics and Motion Control*

Conference; 10 February 2006;
Portoroz, Slovenia. pp. 282-286. DOI:
10.1109/EPEPEMC.2006.4778413

[27] Inoue Y, Yamada K, Morimoto S,
Sanada M. Effectiveness of voltage error
compensation and parameter
identification for model-based
sensorless control of IPMSM. IEEE
Transactions on Industry Applications.
2009;**45**(1):213-221. DOI: 10.1109/
TIA.2008.2009617

[28] Mink F, Kubasiak N, Ritter B,
Binder A. Parametric model and
identification of PMSM considering the
influence of magnetic saturation. In:
13th International Conference on
Optimization of Electrical and
Electronic Equipment. 24–26 May 2012;
Brasov, Romania; 2012. pp. 444-452.
DOI: 10.1109/OPTIM.2012.6231768

[29] Senjyu T, Kinjo K, Urasaki N,
Uezato K. Parameter measurement for
PMSM using adaptive identification. In:
Industrial Electronics, 2002. ISIE 2002.
Proceedings of the 2002 IEEE
International Symposium; 3. pp. 711-716

[30] Tolochko OI, Bozhko VV.
Inductances identification of IPMSM by
the recurrent method of least squares.
Scientific papers of Donetsk National
Technical University. Series: Electrical
engineering and power engineering;
2012;**12**(2):234-238

[31] Trandafilov VN, Bozhko VV,
Tolochko OI. Inertia identification of
electric drive by an unnormalized
gradient method. Scientific papers of
Donetsk National Technical University.
Series: Electrical engineering and power
engineering. 2012;**10**(180):194-199